Compact Distributed RLC Interconnect Models—Part II: Coupled Line Transient Expressions and Peak Crosstalk in Multilevel Networks

Jeffrey A. Davis and James D. Meindl, *Life Fellow, IEEE*

***Abstract*—Novel compact expressions that describe the transient response of high-speed resistance, inductance, and capacitance (rlc) coupled interconnects are rigorously derived. These new distributed rlc models reveal that peak crosstalk voltage is over 60% larger for 3 GHz high-speed interconnects than predicted by current distributed rc models. Simplified forms of the compact models enable physical insight and accurate estimation of peak crosstalk voltage between two and three distributed rlc interconnects.**

***Index Terms*—Crosstalk, inductance, interconnections, time domain analysis, transmission line theory.**

I. Introduction

INTERCONNECT models must incorporate distributed self and mutual inductance to accurately estimate interconnect time delay and crosstalk in a multilevel network for multi-GHz gigascale integration (GSI) [1]. Compact expressions for worst-case time delay and crosstalk of coupled, distributed resistance capacitance (rc) lines are rigorously derived by Sakurai in [2]. This paper significantly extends his expressions to include self and mutual inductance in models of high-speed coupled interconnects for GSI. Novel compact expressions for transient response describe the worst-case time delay and crosstalk of two and three coupled, distributed resistance, inductance, and capacitance (rlc) interconnect models of high-speed, on-chip interconnects. These compact distributed rlc models are used to project the impact of inductance on 3 GHz multilevel interconnect networks implemented with copper and a low κ (~2.0) dielectric material. The models are also used to illustrate the effects of interconnect length and driver impedance on crosstalk, and new closed-form expressions are developed that describe the peak crosstalk voltage for two and three coupled distributed rlc lines.

II. Transient Voltage of Coupled Distributed rlc Interconnects

The partial differential equations (PDE's) that Sakurai solves in [2] and the PDE's that are solved in this paper appear in Fig. 1. In this section, the transient response of a single distributed rlc line is excerpted from a companion paper [3]. From this solution, the transient responses for two and three coupled interconnects are determined.

A. Single Distributed RLC Interconnect

The solution to the single distributed rlc line is rigorously derived in a companion paper [3]. The expressions for a single finite line are presented here for convenient reference. An efficient representation of the distributed rlc expressions for the semi-infinite and finite single line is performed in terms of a generating function, $V_{gen}(x, t, m)$, which has the form in (1), shown at the bottom of the next page. Using this function, the transient solution at a position x along a semi-infinite line is [3]

$$V_{\text{inf}}(x, t) = V_{gen}(x, t, m = 0) \tag{2}$$

and the transient solution at the end of a finite line with length ℓ is given by [3]

$$V_{fin}(\ell, t) = 2V_{gen}(x = \ell, t, m = 0) + 2e^{-(r/2l)t} \sum_{n=1}^{q} \sum_{i=0}^{n} \cdot \sum_{j=0}^{\infty} \frac{n(n-1+j)!}{i!j!(n-i)!} (-1)^i \Gamma^{n-i+j} V_{gen} \cdot (x = (2n+1)\ell, t, m = i+j). \tag{3}$$

B. Two Coupled Distributed RLC Interconnects

The PDEs that describe two coupled distributed rlc interconnects are given by

$$\frac{\partial^2}{\partial x^2} V_Q(x, t) = r(c_{grd} + c_m) \frac{\partial}{\partial t} V_Q(x, t) - rc_m \frac{\partial}{\partial t} V_A(x, t) + (l_s(c + c_m) - l_m c_m) \cdot \frac{\partial^2}{\partial t^2} V_Q(x, t) + (l_m(c_{grd} + c_m) - l_s c_m) \cdot \frac{\partial^2}{\partial t^2} V_A(x, t) \tag{4}$$

$$\frac{\partial^2}{\partial x^2} V_A(x, t) = r(c_{grd} + c_m) \frac{\partial}{\partial t} V_A(x, t) - rc_m \cdot \frac{\partial}{\partial t} V_Q(x, t) + (l_s(c_{grd} + c_m) - l_m c_m) \cdot \frac{\partial^2}{\partial t^2} V_A(x, t) + (l_m(c_{grd} + c_m) - l_s c_m) \cdot \frac{\partial^2}{\partial t^2} V_Q(x, t) \tag{5}$$

Manuscript received September 20, 1999; revised May 2, 2000. This work was supported by the Semiconductor Research Corporation (SJ-374.002) and the Defense Advance Research and Projects Agency (BAA9415-A-009). The review of this paper was arranged by Editor J. M. Vasi.

The authors are with the School of Electrical and Computer Engineering, Georgia Institute of Technology, Atlanta, GA 30332-0250 USA (e-mail: jeff.davis@ece.gatech.edu).

Publisher Item Identifier S 0018-9383(00)09634-9.

0018–9383/00$10.00 © 2000 IEEE

Sakurai's RC Partial Differential Equations

$$\frac{\partial^2}{\partial x^2}V_Q(x,t) = r(c_{grd}+c_m)\frac{\partial}{\partial t}V_Q(x,t) - rc_m\frac{\partial}{\partial t}V_A(x,t)$$

$$\frac{\partial^2}{\partial x^2}V_A(x,t) = r(c_{grd}+c_m)\frac{\partial}{\partial t}V_A(x,t) - rc_m\frac{\partial}{\partial t}V_Q(x,t)$$

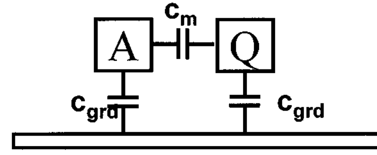

RLC Partial Differential Equations

$$\frac{\partial^2}{\partial x^2}\begin{bmatrix}V_1(x,t)\\V_2(x,t)\\V_3(x,t)\end{bmatrix} = r\begin{bmatrix}2c_{grd}+c_m & -c_m & 0\\ -c_m & 2c_{grd}+2c_m & -c_m\\ 0 & -c_m & 2c_{grd}+c_m\end{bmatrix}\frac{\partial}{\partial t}\begin{bmatrix}V_1(x,t)\\V_2(x,t)\\V_3(x,t)\end{bmatrix} + \begin{bmatrix}l_{11} & l_{12} & l_{13}\\ l_{12} & l_{22} & l_{23}\\ l_{13} & l_{23} & l_{33}\end{bmatrix}\begin{bmatrix}2c_{grd}+c_m & -c_m & 0\\ -c_m & 2c_{grd}+2c_m & -c_m\\ 0 & -c_m & 2c_{grd}+c_m\end{bmatrix}\frac{\partial^2}{\partial t^2}\begin{bmatrix}V_1(x,t)\\V_2(x,t)\\V_3(x,t)\end{bmatrix}$$

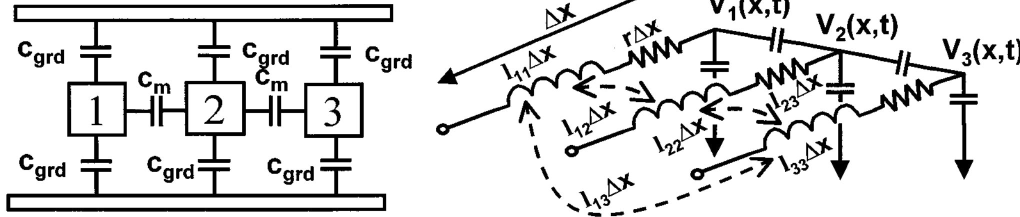

Fig. 1. Partial differential equations solved with Sakurai's distributed rc models and with new compact distributed rlc models

where

- V_A transient voltage along an active line;
- V_Q transient voltage along a quiet line;
- c_{grd} line-to-ground capacitance;
- c_m line-to-line capacitance;
- l_s self-inductance;
- l_m mutual inductance between the two conductors.

Using a transformation similar to [2], which comes from the addition and subtraction of (4) and (5), gives the following set of decoupled PDEs:

$$\frac{\partial^2}{\partial x^2}V_+(x,t) = (l_s+l_m)c\frac{\partial^2}{\partial t^2}V_+(x,t) + rc\frac{\partial}{\partial t}V_+(x,t) \quad (6)$$

$$\frac{\partial^2}{\partial x^2}V_-(x,t) = (l_s-l_m)(c+2c_m)\frac{\partial^2}{\partial t^2}V_-(x,t) + r(c+2c_m)\frac{\partial}{\partial t}V_-(x,t) \quad (7)$$

where $V_+ = V_Q + V_A$ and $V_- = V_A - V_Q$.

The boundary conditions for V_+ and V_- are determined from the boundary conditions of the active and quiet line at $x = 0$ which are given by

$$V_{\text{in}}(t) - R_{\text{tr}}I_A(x=0,t) = V_A(x=0,t) \quad (8)$$

$$-R_{\text{tr}}I_Q(x=0,t) = V_Q(x=0,t). \quad (9)$$

Adding and subtracting these boundary conditions leads to

$$V_{\text{in}}(t) - R_{\text{tr}}I_+(x=0,t) = V_+(x=0,t) \quad (10)$$

$$V_{\text{in}}(t) - R_{\text{tr}}I_-(x=0,t) = V_-(x=0,t). \quad (11)$$

Likewise, the boundary conditions of the active and quiet line at $x = \ell$ are

$$I_A(x=\ell,t) = 0 \quad (12)$$

$$I_Q(x=\ell,t) = 0. \quad (13)$$

Adding and subtracting these boundary conditions gives

$$I_+(x=\ell,t) = 0 \quad (14)$$

$$I_-(x=\ell,t) = 0 \quad (15)$$

$$V_{gen}(x,t,m) = V_{dd}\left(\frac{Z_o}{R_{\text{tr}}+Z_o}\left(\frac{t-x\sqrt{lc}}{t+x\sqrt{lc}}\right)^{m/2} e^{(-rt/2l)}I_0\left[\frac{r}{2l}\sqrt{t^2-\left(x\sqrt{lc}\right)^2}\right] + \frac{1}{2}\sum_{k=1}^{\infty}\left(\frac{t-x\sqrt{lc}}{t+x\sqrt{lc}}\right)^{(k+m)/2} e^{-(rt/2l)}I_{(k+m)}\left[\frac{r}{2l}\sqrt{t^2-\left(x\sqrt{lc}\right)^2}\right](4-\Gamma^{k-1}(\Gamma+1)^2)\right) \cdot u\left[t-x\sqrt{lc}\right]. \quad (1)$$

where I_+ and I_- are the plus and minus modes of the current and are completely analogous to the voltage plus and minus modes.

Therefore, from (10), (11), (14), and (15) and the boundary conditions for the plus and minus transformation are the same as the boundary conditions of a single line driven by a step input function with an arbitrary source impedance and an open-circuit load.

The plus and minus modes have physical interpretations as being the solutions to the coupled line configuration with two different initial conditions. The plus mode, for example, has the interpretation that it is the solution to the voltage of either line when both are excited simultaneously. The effective capacitance of the plus mode is, therefore, the line-to-ground capacitance because by definition the potential between the lines is zero. The currents in this plus configuration are in the same direction; therefore, the magnetic flux emanating from each line is in the same direction in the orthogonal surface linking each conductor to the ground plane. For this configuration, the effective flux linkage of each line is increased which produces a higher effective inductance for the plus mode. This is evident in the partial differential equations for the plus mode in that the effective inductance is the self-inductance plus the mutual inductance.

The minus mode is the solution to the transient response of the active line when the adjacent line is switching with opposite polarity. Because of the Miller effect, the mutual capacitance is effectively twice its original value. This is evident in the PDE for the minus mode that has an effective capacitance equal to the line-to-ground capacitance plus *twice* the mutual capacitance. In addition, the currents in this configuration are equal in magnitude and opposite in direction. The magnetic fluxes emanating from each line are in opposing directions. The effective flux linkage of each line is, therefore, reduced which produces an effectively lower inductance. This is evident in the PDE for the minus mode that has an effective inductance equal to the self-inductance minus the mutual inductance.

The worst-case time delay occurs when the two-coupled lines are switching with opposite polarity. As mentioned, the transient solution for this configuration is equal to the minus mode solution, which is

$$V_A(\ell, t) = V_{fin}(\ell, t, l = l_s - l_m, c = c_{grd} + 2c_m) \quad (16)$$

where $V_{fin}(x, t)$ is defined in (3).

The transient response of the worst-case crosstalk occurs when both lines are initially uncharged and the active line charges to V_{dd}. Under these worst-case crosstalk conditions, the transient response on the quiet line is

$$\begin{aligned} V_Q(\ell, t) = \tfrac{1}{2}(&V_{fin}(\ell, t, l = l_s + l_m, c = c_{grd}) \\ &- V_{fin}(\ell, t, l = l_s - l_m, c = c_{grd} + 2c_m)) \end{aligned} \quad (17)$$

where $V_{fin}(x, t)$ is defined in (3).

C. Three Coupled Distributed RLC Interconnects

In this section, the expressions for the worst-case time delay and crosstalk of three parallel interconnects sandwiched between two virtual ground planes are derived. Each line has arbitrary source impedance, $R_{\rm tr}$, and an open-circuit load termination. The expressions for the capacitance and inductance matrices of three-coupled interconnects are determined using compact quasi-analytical expressions [4] combined with a quasi-TEM wave analysis [5]. The quasi-TEM wave analysis gives the following relationship between the capacitance and inductance matrix:

$$[L][C] = \frac{1}{\nu^2}[I] \quad (18)$$

where v is the speed of an electromagnetic wave in a given dielectric material, and $[I]$ is the unity matrix with all diagonal elements equal to one and off-diagonal elements equal to zero. Physically, (18) assumes a perfect return path is present in the virtual ground planes that are above and below the three-coupled interconnects. Because of this idealization, the models describe in this paper project a lower limit on the crosstalk voltage and time delay.

The partial differential equations that describe the three conductor two ground plane model are then given by

$$\begin{aligned} &\frac{\partial^2}{\partial x^2}\begin{bmatrix} V_1(x, t) \\ V_2(x, t) \\ V_3(x, t) \end{bmatrix} \\ &= r\begin{bmatrix} c_{grd}+c_m+c_{13} & -c_m & -c_{13} \\ -c_m & c_{grd}+2c_m & -c_m \\ -c_{13} & -c_m & c_{grd}+c_m+c_{13} \end{bmatrix} \\ &\cdot \frac{\partial}{\partial t}\begin{bmatrix} V_1(x, t) \\ V_2(x, t) \\ V_3(x, t) \end{bmatrix} + \frac{1}{\nu^2}\frac{\partial^2}{\partial t^2}\begin{bmatrix} V_1(x, t) \\ V_2(x, t) \\ V_3(x, t) \end{bmatrix}. \end{aligned} \quad (19)$$

It is assumed that the two outer conductors always have the same potential. To emphasize this point a new notation is adopted, which is

$$V_i(x, t) = V_2(x, t) \quad (20)$$

$$V_o(x, t) = V_1(x, t) = V_3(x, t) \quad (21)$$

where $V_i(x, t)$ is voltage on the inner conductor and $V_o(x, t)$is voltage on the outer conductors. The three equations in (19) reduce to

$$\begin{aligned} &\frac{\partial^2}{\partial x^2}V_o(x, t) \\ &\quad = r(c_{grd} + c_m)\frac{\partial}{\partial t}V_o(x, t) - rc_m\frac{\partial}{\partial t}V_i(x, t) \\ &\qquad + \frac{1}{\nu^2}\frac{\partial^2}{\partial t^2}V_o(x, t) \end{aligned} \quad (22)$$

$$\begin{aligned} &\frac{\partial^2}{\partial x^2}V_i(x, t) \\ &\quad = -2rc_m\frac{\partial}{\partial t}V_o(x, t) - r(c_{grd} + 2c_m)\frac{\partial}{\partial t}V_i(x, t) \\ &\qquad + \frac{1}{\nu^2}\frac{\partial^2}{\partial t^2}V_i(x, t) \end{aligned} \quad (23)$$

$$\begin{aligned} &\frac{\partial^2}{\partial x^2}V_o(x, t) \\ &\quad = r(c_{grd} + c_m)\frac{\partial}{\partial t}V_o(x, t) - rc_m\frac{\partial}{\partial t}V_i(x, t) \\ &+ \frac{1}{\nu^2}\frac{\partial^2}{\partial t^2}V_o(x, t). \end{aligned} \quad (24)$$

The coupling capacitance between the first and third conductor, c_{13}, is absent in the above three differential equations. Physically c_{13} disappears because the outer two lines are held at the same potential by definition; therefore, the capacitance between them never charges and does not affect the transient characteristics of $V_i(x, t)$ or $V_o(x, t)$.

Also, (22) is identical to (24), and, therefore, the two independent equations are (22) and (23). To decouple these two equations, first add (23) to twice (22), which leads to

$$\frac{\partial^2}{\partial x^2}(2V_o + V_i) = rc_{grd}\frac{\partial}{\partial t}(2V_o + V_i) + \frac{1}{\nu^2}\frac{\partial^2}{\partial t^2}(2V_o + V_i). \tag{25}$$

Also consider the difference of (23) and (22), which gives

$$\frac{\partial^2}{\partial x^2}(V_o - V_i) = r(c_{grd} + 3c_m)\frac{\partial}{\partial t}(V_o - V_i) + \frac{1}{\nu^2}\frac{\partial^2}{\partial t^2} \cdot (V_o - V_i). \tag{26}$$

Both these operations reveal new transformation variables that are defined as

$$V_{sum} = 2V_o + V_i \tag{27}$$

$$V_{diff} = V_o - V_i. \tag{28}$$

Using the transformation in (27) and (28) on the boundary conditions of the inner and outer interconnects gives the boundary condition of the sum and difference mode at $x = 0$ as

$$2V_{\text{in}}(t) = V_{sum}(x = 0) + R_{\text{tr}}I_{sum}(x = 0) \tag{29}$$

$$V_{\text{in}}(t) = V_{diff}(x = 0) + R_{\text{tr}}I_{diff}(x = 0). \tag{30}$$

The boundary conditions of the sum and difference mode at $x = \ell$ are given by

$$I_{sum}(x = \ell) = 0 \tag{31}$$

$$I_{diff}(x = \ell) = 0. \tag{32}$$

The sum and difference modes have transient solutions that are identical to single line solutions with different capacitance and inductance values. These single line sum and difference mode solutions are used to determine the worst-case crosstalk and time delay transient response of the three-coupled interconnects. For example, the worst-case crosstalk occurs when all three lines are initially low, and the two outer interconnects are simultaneously active. Using the transformations and boundary conditions outlined in this section, the transient expression for the worst case crosstalk on the inner interconnect is

$$V_Q(\ell, t) = \frac{2}{3}\left(V_{fin}\left(\ell, t, l = \frac{1}{2c_{grd}\nu^2}, c = 2c_{grd}\right) - V_{fin}\left(\ell, t, l = \frac{1}{(2c_{grd} + 3c_m)\nu^2}, c = 2c_{grd} + 3c_m\right)\right). \tag{33}$$

The worst-case time delay occurs when the inner line switches with an opposite polarity of the outer two lines. Changing the initial conditions and boundary conditions slightly in the analysis in this section so that the inner line is active and the outer lines are discharging gives the transient response of the worst-case time delay of the active line to be

$$V_A(\ell, t) = \frac{4}{3}V_{fin}\left(\ell, t, l = \frac{1}{(2c_{grd} + 3c_m)\nu^2}, c = 2c_{grd} + 3c_m\right) - \frac{1}{3}V_{fin}\left(\ell, t, l = \frac{1}{2c_{grd}\nu^2}, c = 2c_{grd}\right). \tag{34}$$

D. HSPICE Verification of Compact Expressions

To verify these new compact expressions, Fig. 2(a)–(d) compares the compact model predictions to an HSPICE simulation of 1, 10, 50, and 500 lumped RLC elements. Fig. 2 illustrates that as the number of lump elements increases the HSPICE simulations converge to the distributed rlc solution. In addition, unlike HSPICE the compact expressions can be used with various searching algorithms to calculate directly without intermediate steps interconnect characteristics such as peak crosstalk voltage, time delay, and overshoot.

Physical insight gained by the derivation of new compact expressions is explored in the following sections by examining the design of a 3 GHz interconnect bus.

III. 3 GHz Global Bus Example for 2012

To illustrate the effects of inductance on multilevel wiring network architectures for GSI, a National Technology Roadmap for Semiconductors (NTRS) case study is investigated. Technology constraints for a high-speed application specific integrated circuit (ASIC) at 2012 are projected by the NTRS [6] to have: a chip area of 13 cm^2, a global clock frequency of 3 GHz, a local clock frequency of 10 GHz, a low k (∼2.0) interlevel dielectric, and copper metal technology. This section introduces salient inductive effects for future high-speed interconnect networks and explores the design of a 3 GHz high-speed die-edge-length interconnect using single driver and repeater circuits.

A. Single Driver Global Interconnect Design

To initiate the investigation of inductive effects, a 3 GHz die-edge-length single driver interconnect circuit is examined. This interconnect circuit might be desirable for the initial design of an ASIC high-speed bus connecting predesigned and tested macrocells cores from a variety vendors in which repeaters cannot be easily inserted without costly core redesign. These single driver circuits, therefore, provide a global bus design for an ASIC system-on-a-chip (SOC) that potentially reduces time-to-market.

The 3 GHz die-edge-length interconnect bus of this case study is first designed using a distributed rc model [2]. The drivers of this global interconnect bus are assumed to have an output resistance much less than the wire resistance, and each cross-sectional dimension of the 3 GHz wiring level is assumed to be approximately equal. The cross-sectional dimensions are computed so that a die-edge-length interconnect (3.6 cm) on the 3 GHz wiring levels has a maximum time delay of 300 ps and a maximum crosstalk of $0.2V_{dd}$. Using rc models, the condition that all cross-sectional dimensions are equal satisfies the

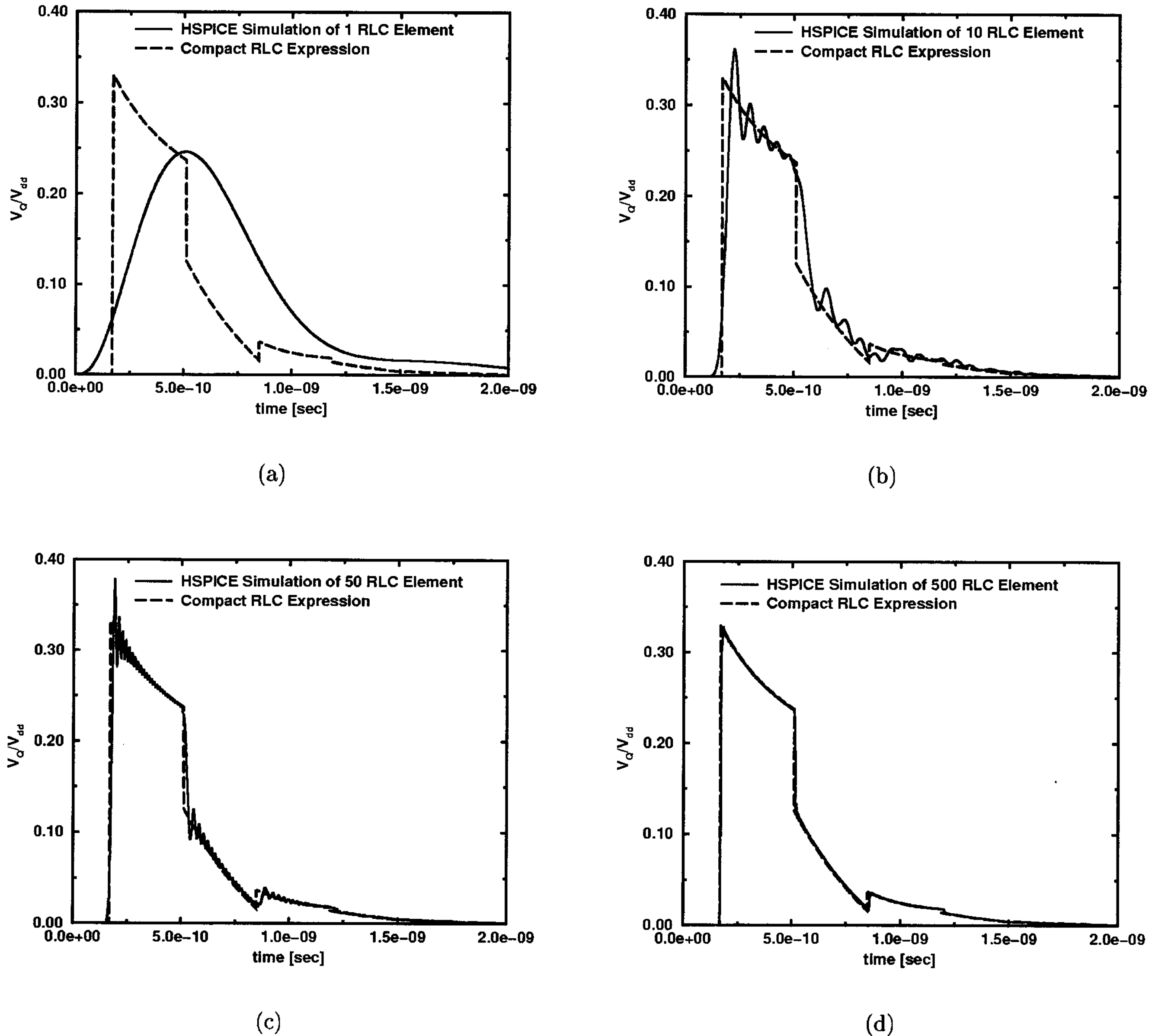

Fig. 2. Compact rlc model compared to HSPICE simulation of (a) 1, (b) 2, (c) 3, and (d) 500 lumped rlc elements ($Z_o^- = 88.77\ \Omega$, $Z_o^+ = 266.32\ \Omega$, $R_{\rm tr} = 133.3\ \Omega$, $r = 37.86\ \Omega$/cm, $L = 3.6$ cm).

TABLE I
RC DESIGN OF A 3 GHz TIER

Physical Parameter	RC Models Predict	Compact RLC Models Predict	Percent Difference
Peak Crosstalk	$0.195V_{dd}$	$0.317V_{dd}$	62.56%
Time Delay	302.3ps	315.0ps	4.2%

crosstalk constraint, and the time delay constraint is met by using the following rc expression to calculate the interconnect dimensions:

$$300\text{ ps} = 0.4r(2c_{grd} + 4c_m)\ell^2 = \frac{0.4\rho(17.87)\varepsilon_o}{W^2}\,\ell^2 \quad (35)$$

where

ρ resistivity of copper;

ε_o permittivity of free space;

W primary wire cross-sectional dimension.

As seen in Table I, *peak crosstalk voltage with the rlc model is 62.5% larger for the 3 GHz global interconnect, than with the rc model.* Fig. 3 compares the marked differences between the worst-case time delay waveforms and the worst-case crosstalk waveforms between three coupled lines using a distributed rlc model and distributed rc models for the 3 GHz interconnect bus.

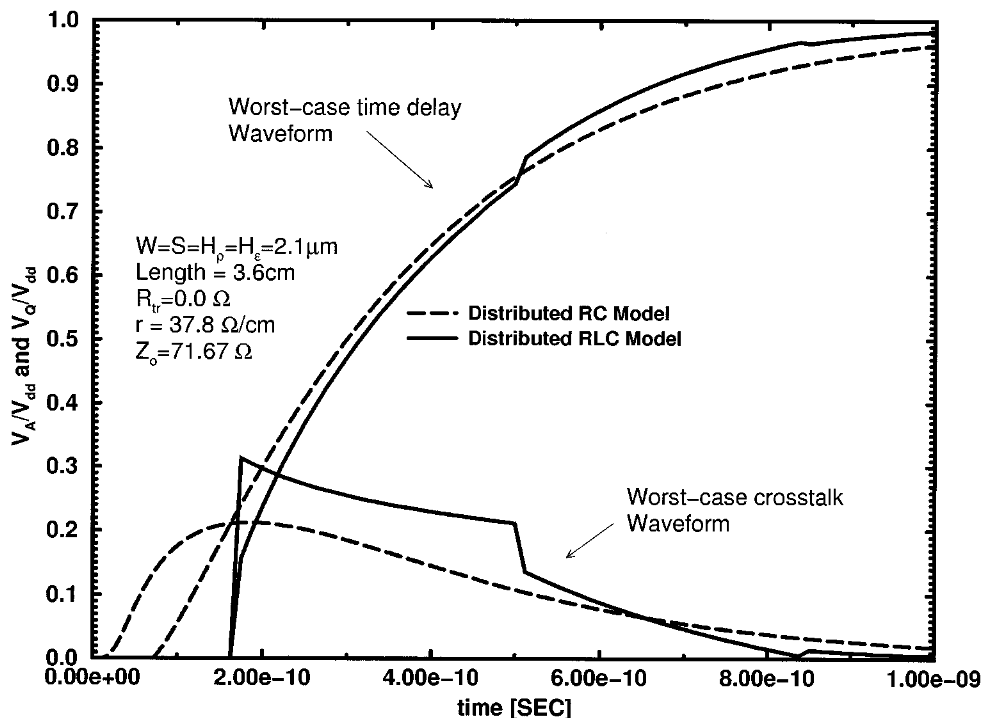

Fig. 3. Transient waveforms for a 3 GHz die-edge-length interconnect using distributed rc and distributed rlc models

TABLE II
RLC REDESIGN OF A 3 GHz TIER

Physical Parameter	RC Design	Compact RLC Re-Design	Percent Difference
$W=H_\rho=H_\varepsilon$	2.1micron	2.1micron	-
S	2.1micron	2.95micron	40.47%

To reduce the peak crosstalk voltage on these global interconnects, the interconnect spacing is increased until the compact distributed rlc models predict that the peak crosstalk voltage equals $0.2V_{dd}$. *To reduce rlc model crosstalk to 0.2 V_{dd},* 40.5% *larger spacing is required for the 3 GHz tier than for the rc model as seen in Table II.*

B. Global Interconnect Repeater Insertion

Incorporating repeaters to increase wire density and global communication bandwidth is used to further optimize the SOC product outlined in the previous section. This section, therefore, introduce the effects that inductance has on the transient characteristics of a 3 GHz die-edge-length interconnect with repeaters. This repeater interconnect circuit is designed using distributed rc models, and it is analyzed using the distributed rlc models. A redesign of this example using distributed rlc models is also discussed.

For this example, it is assumed that a die-edge length interconnect has a time delay of 300 ps and a maximum crosstalk of 0.2 V_{dd}. It is also assumed that *ten* repeaters are inserted along the die-edge-length interconnects to increase wire density. This number of repeaters is used in this example because ten repeaters provide a significant increase in wire density with a tolerable number of repeaters per interconnect. The driver size is optimized using distributed rc models from [7], and the optimal driver scaling factor, h, is given by

$$h = \sqrt{\frac{R_o(2c_{grd} + 4c_m)}{rC_o}} \tag{36}$$

where

R_o minimum size driver output resistance;
C_o minimum size driver input capacitance;
r distributed resistance per unit length;
c_{grd} and c_m distributed line-to-ground and line-to-line capacitance per unit length, respectively.

In addition, time delay of this repeater circuit is given by [7] as

$$\tau = 0.7R_oC_ok + 1.4L\sqrt{R_oC_or(2c_{grd} + 4c_m)} + \frac{0.4r(2c_{grd} + 4c_m)L^2}{k}. \tag{37}$$

where k is the number of repeaters segments. Setting (37) equal to 300 ps and solving for the interconnect width gives a value of 0.72 μm. The insertion of these repeaters, therefore, increases the wire density by approximately a factor of three.

This distributed rc repeater design is now analyzed using the new compact distributed rlc model. The models derived in this paper are used to analyze this repeater circuit because the wire capacitance (553.72 fF) is more than an order of magnitude greater than the load capacitance (30.8 fF) of each repeater seg-

TABLE III
RC DESIGN OF A 3 GHz REPEATER TIER

Physical Parameter	RC Models Predict	Compact RLC Models Predict	Percent Difference
Peak Crosstalk	$0.2V_{dd}$	$0.323V_{dd}$	61.5%
Time Delay	27.7ps	29.4ps	6.12%

TABLE IV
RLC RE-DESIGN OF A 3 GHz REPEATER TIER

Physical Parameter	RC Design	Compact RLC Re-Design	Percent Difference
$W=H_\rho=H_\varepsilon$	0.73micron	0.73micron	-
S	0.73micron	1.05micron	43.8%

ment and to first order is ignored. As seen in Table III, *peak crosstalk voltage with the distributed rlc model is 61.5% larger for the 3 GHz global interconnects, than with the distributed rc model. Moreover, in order to reduce rlc model crosstalk to 0.2 V_{dd}*, 44.2% *larger spacing is required than for the rc model as seen in Table IV.*

Even though repeater circuits significantly increase wire density, repeater insertion in this example did not mitigate the impact of inductance. Further investigation into the effects of inductance on repeater circuit design is warranted, however, because in aggressive repeater circuits with high repeater counts the interaction between the inductance and load capacitance cannot be ignored.

C. Optimal Global Interconnect Cross-Sectional Dimension

To conclude the discussion of this 3 GHz global wiring example, the assumption that all cross-sectional dimensions are equal is relaxed in this section. Given the constraints that the maximum metal height to metal width ratio at 2012 is 3 [6], the maximum time delay of a 0.36 cm length repeater section is 30 ps, and the maximum crosstalk is 0.2 V_{dd}, the cross-sectional dimensions are calculated to find the minimum pitch that meets these design constraints.

Because of the computational efficiency of the new compact expressions, the time delay and crosstalk for a large number of possible cross-sectional designs is quickly calculated to search for the optimal dimensions *that minimize wire pitch.* The optimal dimensions that minimize the wire pitch for the 3 GHz interconnects are given in Table V. The first observation of this optimal design is that the maximum metal height to width ratio of 3.0 is used. In addition, the wire spacing is 60% larger than the metal width, and the dielectric thickness is 20% of the metal height. This small dielectric thickness is due to the maximum crosstalk constraint. Increasing the dielectric thickness decreases the time delay, but increases the crosstalk beyond 0.2 V_{dd}.

Table V also compares the optimal values of cross-sectional dimension to the dimensions calculated in the previous section. This optimal scaling methodology decreases the wire pitch of the global bus from the previous section by 27%.

IV. DEPENDENCE OF INDUCTIVE CROSSTALK ON INTERCONNECT LENGTH AND DRIVER DESIGN

If a distributed rc interconnect is driven by a step input excitation voltage, then peak crosstalk between symmetric coupled lines is approximately length independent [2]. The incorporation of inductance, however, introduces a *nonlinear length dependence of crosstalk* for global GSI interconnects as seen in Fig. 4 for three different source impedance values in a 3 GHz wiring level. The most striking feature of Fig. 4 is that maximum crosstalk occurs for wire lengths *shorter* than the die-edge-length (3.6 cm) for the single driver example outlined in the previous section. This is due to the larger total lumped resistance of the die-edge-length and longer interconnects that cause inductive crosstalk to attenuate.

TABLE V
OPTIMAL INTERCONNECT DESIGN WITH THE INCLUSION OF INDUCTANCE

Interconnect Parameter	Optimal Value	Previous Value
Source Resistance	6.24 Ohms	6.24 Ohms
Metal Width	0.5 micron	0.73 micron
Metal Thickness	1.5 micron	0.73 micron
Dielectric Thickness	0.3 micron	0.73 micron
Metal Spacing	0.8 micron	1.05 micron
Metal Pitch	1.3 micron	1.78 micron
Time Delay	29.5ps	29.4ps
Peak Crosstalk	$0.2V_{dd}$	$0.2V_{dd}$

CMOS driver design for the 3 GHz global wiring level is significantly influenced by inductance. For example, driver design has a pronounced effect on interconnect crosstalk as seen by comparing Fig. 5(a)–(c). Increasing cumulative interconnect and driver resistance decreases peak crosstalk voltages to the rc predicted values at the cost of larger interconnect time delay. For example, the interconnect in Fig. 5(c) with a larger driver resistance has a time delay that is 3.7 times larger than the time delay of the interconnect in Fig. 5(a). The reduction in crosstalk illustrated in Fig. 5 is due to the fact that extra circuit resistance effectively masks inductive effects. For fixed interconnect dimensions, therefore, an interconnect driver should have an output impedance that enables full utilization of the interconnect time delay budget so as to reduce peak inductive crosstalk.

V. APPROXIMATE EXPRESSION FOR PEAK CROSSTALK

The new compact expressions in (17) and (33) provide the basis for efficient computation of inductive effects for coupled distributed rlc interconnects. Further simplification, however, is necessary to improve physical understanding of rlc crosstalk as well as immediate calculation.

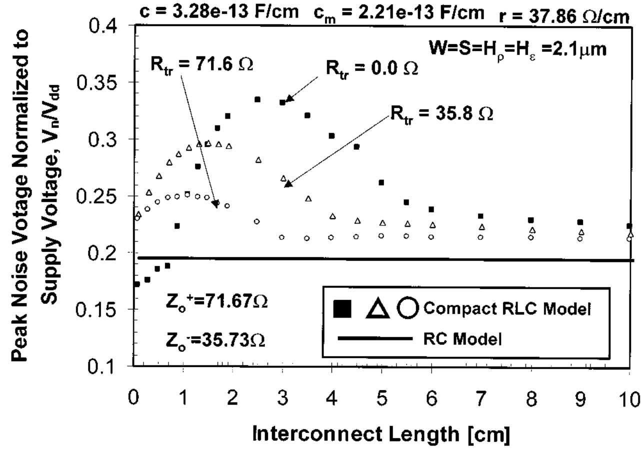

Fig. 4. Length dependence of crosstalk reveal using new compact models for three values of the driver source resistance

To find an approximate peak crosstalk expression, the plus and minus modes for two or three coupled semi-infinite interconnects are approximated as low-loss transmission line solutions. The transient solutions at a position x, therefore, are

$$\frac{V_+(x,t)}{V_{dd}} = \frac{Z_o^+}{Z_o^+ + R_{\text{tr}}}\, e^{-(rx/2Z_o^+)} u\left(t - \frac{x}{\nu}\right) \tag{38}$$

and

$$\frac{V_-(x,t)}{V_{dd}} = \frac{Z_o^-}{Z_o^- + R_{\text{tr}}}\, e^{-(rx/2Z_o^-)} u\left(t - \frac{x}{\nu}\right) \tag{39}$$

where $Z_o^+ = \sqrt{(l_s + l_m)/c_{grd}}$ and $Z_o^- = \sqrt{(l_s - l_m)/(c_{grd} + 2c_m)}$ are the lossless characteristic impedances of the plus and minus modes for two coupled lines over a single ground plane, or $Z_o^+ = 1/(\nu 2c_{grd})$ and $Z_o^- = 1/v(2c_{grd} + 3c_m)$ are the lossless characteristic impedances of the sum and difference modes for three coupled lines between two ground planes.

Equations (38) and (39) are plotted as a function of position in Fig. 6. One key feature of Fig. 6 is that there is an interconnect length for which the difference between these two modes is a maximum. This difference is significant because it is proportional to the quiet line voltage.

For a finite line, it is assumed that the peak noise voltage occurs at the first reflection as seen in Fig. 5(a). The semi-infinite line low-loss solutions, therefore, are doubled at the end of the line because it has an open circuit termination. Likewise, when the interconnects are long ($\ell \gg Z_o/r$), the interconnect total resistance is so great that inductive effects are suppressed, and the distributed rc model become valid [2]. Therefore, an approximate closed-form expression for the peak crosstalk voltage for distributed rlc interconnects is piecewise defined as

Region I: $\ell \leq \ell_{crit}$

$$\frac{V_{peak}}{V_{dd}} = \chi\left(\frac{Z_o^+}{Z_o^+ + R_{\text{tr}}}\, e^{-(r\ell/2Z_o^+)} - \frac{Z_o^-}{Z_o^- + R_{\text{tr}}}\, e^{-(r\ell/2Z_o^-)}\right) \tag{40}$$

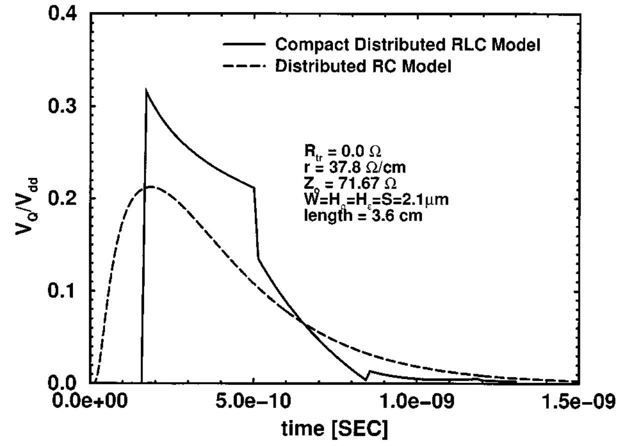

(a)

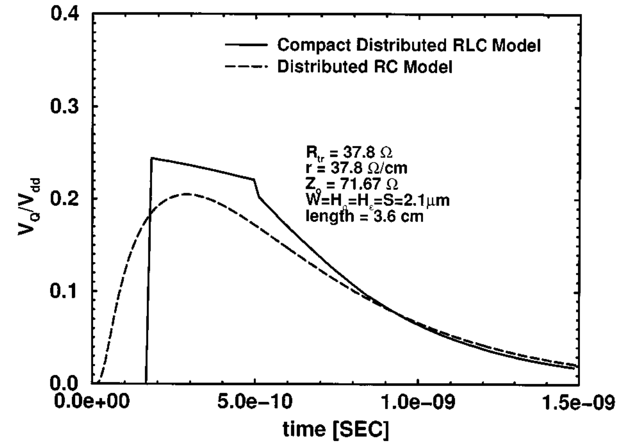

(b)

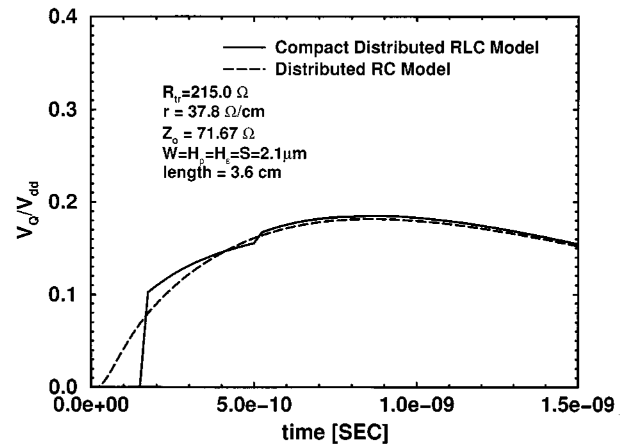

(c)

Fig. 5. Worst-case crosstalk for a 3 GHz die-edge-length interconnect with a driver resistance of (a) 0.0 Ω, (b) 37.8 Ω, and (c) 215 Ω.

$$\Bigg(\text{e.g., for two lines}$$

$$\frac{V_{peak}}{V_{dd}} = \left(\frac{1}{1 + vc_{grd}R_{\text{tr}}}\, e^{-(r\ell vc_{grd}/2)} - \frac{1}{1 + v(c_{grd} + 2c_m)R_{\text{tr}}}\, e^{-(r\ell(c_{grd}+2c_m)/2)}\right)\Bigg)$$

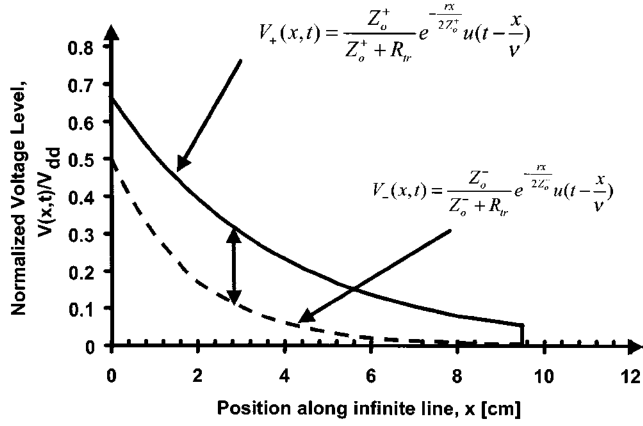

Fig. 6. Plot of the plus and minus modes traveling down a semi-infinite low-loss transmission line.

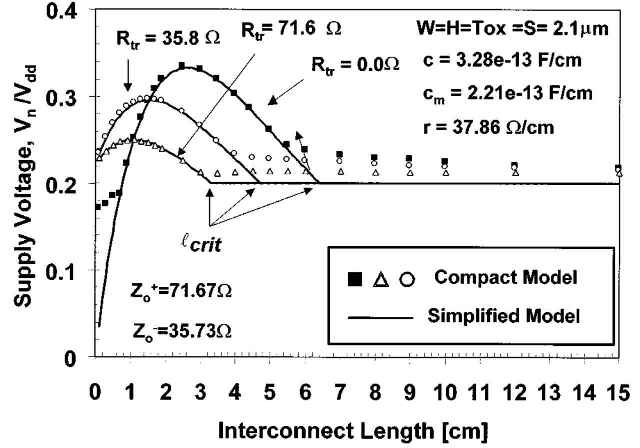

Fig. 7. Simplified closed-form expression compared to compact distributed rlc models as a function of length for three different driver impedances.

Region II: $\ell > \ell_{crit}$

$$\frac{V_{peak}}{V_{dd}} = \frac{1}{2}\,\frac{c_m}{c_{grd} + c_m} \tag{41}$$

where $\chi = 1$, $Z_o^+ = \sqrt{(l_s + l_m)/c_{grd}} = 1/vc_{grd}$, and $Z_o^- = \sqrt{(l_s - l_m)/(c_{grd} + 2c_m)} = 1/v(c_{grd}+2c_m)$ for two-coupled lines, $\chi = 4/3$, $Z_o^+ = 1/\nu 2c_{grd}$, and $Z_o^- = 1/v(2c_{grd} + 3c_m)$ for three-coupled lines, v is the speed of light in a dielectric, and $\ell_{crit}$is determined from the solution of

$$\chi\left(\frac{Z_o^+}{Z_o^+ + R_{\rm tr}}\, e^{-(r\ell_{crit}/2Z_o^+)} - \frac{Z_o^-}{Z_o^- + R_{\rm tr}}\, e^{-(r\ell_{crit}/2Z_o^-)}\right) = \frac{1}{2}\,\frac{c_m}{c + c_m}. \tag{42}$$

This new peak crosstalk expression is compared to results from the compact rlc expression in Fig. 7. Agreement is close in the nonlinear region near maximum V_n/V_{dd} and again in the flat region. In the transition between these two regions, as defined in (40) and (41), the complete compact model is needed to get an accurate estimation of the peak crosstalk.

An approximate expression for ℓ_{crit} comes from the observation that Z_o^+ is always greater than Z_o^-. With significant coupling capacitance the second exponential term in is ignored and $\ell_{crit}$is derived to be

$$\ell_{crit} \approx \frac{2Z_o^+}{r}\,\ln\left[\frac{Z_o^+ 2\chi(c_{grd} + c_m)}{(Z_o^+ + R_{\rm tr})c_m}\right]. \tag{43}$$

This critical length demarks when inductance is important for interconnect crosstalk. In fact, inductive effects can be *ignored* to first order if the following conditions hold:

$$R > 2Z_o^+ \ln\left[\frac{Z_o^+ 2\chi(c_{grd} + c_m)}{(Z_o^+ + R_{\rm tr})c_m}\right] \quad \text{OR}$$
$$R_{\rm tr} > Z_o^+\left(2\chi\,\frac{c_m}{c_{grd}} + (2\chi - 1)\right). \tag{44}$$

Both conditions in (44) come directly from (43). The latter condition is a result of ensuring that the argument of the logarithm in (43) is greater than one.

Using very rudimentary parallel plate models for the capacitance and inductance, the expressions for the peak noise voltage between two parallel lines are

Region I: $\ell \le \ell_{crit}$

$$V_{peak} = \left(\frac{1}{1 + v\left(\frac{\varepsilon W}{H_\varepsilon}\right) R_{\rm tr}}\, e^{-(\rho\ell v\varepsilon/2H_\varepsilon H_\rho)} - \frac{1}{1 + v\varepsilon\left(\frac{W}{H_\varepsilon} + 2\,\frac{H_\rho}{S}\right) R_{\rm tr}} \cdot e^{-\ell\rho v\varepsilon\left((1/2H_\rho H_\varepsilon) + (1/WS)\right)}\right) \tag{45}$$

Region II: $\ell > \ell_{crit}$

$$V_{peak} = \frac{1}{2}\,\frac{1}{1 + \frac{WS}{H_\varepsilon H_\rho}}. \tag{46}$$

Physical insight is gained from the simple models in (45) and (46) by assuming that $R_{\rm tr} = 0$ in (45) which gives

$$V_{peak} = e^{-(\rho\ell c_o\varepsilon_o\sqrt{\varepsilon_r}/2H_\varepsilon H_\rho)}\left(1 - e^{-(\ell\rho c_o\varepsilon_o\sqrt{\varepsilon_r}/WS)}\right). \tag{47}$$

Equation (47) reveals that decreasing the metal (H_ρ) and dielectric thickness (H_ε) decreases total crosstalk, and decreasing the metal width (W) and spacing (S) increases total crosstalk.

The interconnect length at which the peak noise voltage occurs is calculated from setting the derivative of (40) equal to zero, as follows:

$$\frac{dV_{peak}}{d\ell} = \left(-\frac{Z_o^+}{Z_o^+ + R_{\rm tr}}\,\frac{r}{Z_o^+}\, e^{-(r\ell/2Z_o^+)} + \frac{Z_o^-}{Z_o^- + R_{\rm tr}}\,\frac{r}{Z_o^-}\, e^{-(r\ell/2Z_o^-)}\right) = 0. \tag{48}$$

Solving for the length at which this peak occurs gives

$$\ell_{\max} = \frac{2Z_o^- Z_o^+}{r(Z_o^- - Z_o^+)} \ln\left[\frac{(Z_o^- + R_{\rm tr})}{(Z_o^+ + R_{\rm tr})}\right]. \qquad (49)$$

The peak noise at this length is determined from substituting (49) into (48), which gives

$$\frac{V_{peak,\max}}{V_{dd}} = \chi \left[\frac{(Z_o^- + R_{\rm tr})}{(Z_o^+ + R_{\rm tr})}\right]^{-(Z_o^-/(Z_o^- - Z_o^+))} \frac{Z_o^+ - Z_o^-}{Z_o^+ + R_{\rm tr}}. \qquad (50)$$

This is the peak noise voltage for an interconnect wiring level assuming there exists parallel interconnects of length $\ell_{\max}$. For the example presented in Fig. 7, (50) predicts that the peak crosstalk is $0.331V_{dd}$ as compared to the 0.199 V_{dd} as predicted by Sakurai's model for $R_{\rm tr} = 0$.

In fact, assuming that there are two parallel lines and $R_{\rm tr} = 0$ expression (49) and (50) simplify to

$$\ell_{\max} = \frac{1}{vrc_m} \ln\left[\frac{(c_{grd} + 2c_m)}{c_{grd}}\right] \qquad (51)$$

and

$$\frac{V_{peak,\max}}{V_{dd}} = \left(\frac{c_{grd}}{c_{grd} + 2c_m}\right)^{c_{grd}/2c_m} \left(\frac{c_{grd}}{c_{grd} + 2c_m}\right) \frac{2c_m}{c_{grd}} \approx \frac{\pi}{4} \frac{c_m}{c_{grd} + c_m}. \qquad (52)$$

Equation (52) compares directly to Sakurai's full crosstalk expression in [2] and shows that the peak crosstalk at ℓ_{crit} is exactly $2\pi/4 = 1.57$ times larger than predicted by a distributed rc model with zero source impedance.

VI. Conclusion

Compact expressions that describe the transient response of distributed coupled rlc interconnects including worst-case time delay and crosstalk are rigorously derived. These new expressions enhance understanding and computation of inductive effects in a GSI multilevel network. For a 3 GHz global die-edge-length interconnect, the inclusion of inductance

1) increases worst-case peak crosstalk over 60%;
2) requires an increase in the wiring spacing over 40%;
3) introduces a new nonlinear length dependence of peak crosstalk voltage that has a peak that can be up to 1.57× larger than the rc predicted value;
4) reveals the dependence of inductive crosstalk on driver impedance.

Finally, a new closed-form expression for the peak crosstalk voltage on distributed rlc lines is rigorously derived, and it reveals a coupling length at which the maximum peak crosstalk occurs.

References

[1] K. Lee, "On-chip interconnects—Giga hertz and beyond," in *Proc. Int. Interconnect Technology Conf.*, 1998, pp. 15–17.
[2] T. Sakurai, "Closed-form expressions for interconnect delay, coupling, and crosstalk in VLSIs," *IEEE Trans. Electron Devices*, vol. 40, pp. 118–124, Jan. 1993.
[3] J. A. Davis and J. D. Meindl, "Compact distributed RLC models—part I: Single line transient, time delay, and overshoot expressions," *IEEE Trans. Electron Devices*, vol. 47, pp. 2068–2077, Nov. 2000.
[4] J. H. Chern *et al.*, "Multilevel metal capacitance models for CAD design synthesis systems," *IEEE Electron Device Lett.*, vol. 13, pp. 32–34, Jan. 1992.
[5] C. R. Paul, *Analysis of Multi-conductor Transmission Lines*. New York: Wiley, 1994.
[6] Semiconduct. Ind. Assoc., "The National Technology Roadmap for Semiconductors,", San Jose, CA, 1997.
[7] H. B. Bakoglu, *Circuits, Interconnections, and Packaging for VLSI*. Reading, MA: Addison-Wesley, 1990.

Jeffrey A. Davis received the B.E.E., M.S.E.E., and Ph.D. degrees in electrical engineering from the Georgia Institute of Technology (Georgia Tech.) in 1993, 1997, and 1999, respectively.

He joined the faculty at Georgia Tech as an Assistant Professor in 1999, and his current research interests are in the areas of high-speed interconnect modeling and optimization, novel "short-wire" architectures and design methodologies, and optimal multilevel interconnect network design for future GSI processors.

James D. Meindl (M'56–SM'66–F'68–LF'97) received the B.S., M.S., and Ph.D. degrees in electrical engineering from Carnegie Mellon University, Pittsburgh, PA, in 1955, 1956, and 1958, respectively.

He is the Director of the Joseph M. Pettit Microelectronics Research Center and the Pettit Chair Professor of Microelectronics at the Georgia Institute of Technology, Atlanta. Previously, he served from 1986 to 1993 as Senior Vice President for Academic Affairs and Provost of Rensselaer Polytechnic Institute, Troy, NY. From 1967 through 1986, he was with Stanford University, Stanford, CA, where he was John M. Fluke Professor of Electrical Engineering, Associate Dean for Research in the School of Engineering, Director of the Center for Integrated Systems, Director of the Electronics Laboratories, and founding Director of the Integrated Circuits Laboratory. He is co-founder of Telesensory Systems, Inc., the principal manufacturer of electronic reading aids for the blind, and served as a member of the Board from 1971 through 1984. From 1965 through 1967, he was Founding Director of the Integrated Electronics Division at the Fort Monmouth, NJ, U.S. Army Electronics Laboratories. He is author of *Micropower Circuits* and over 300 technical papers on ultralarge-scale integration, integrated electronics, and medical electronics; and editor of *Brief Lessons in High Technology*, which elucidates the most important economic event of our lives, the emergence of the information society. His major contributions have been new medical instruments enabled by custom integrated electronics, projections and codification of the hierarchy of physical limits on integrated electronics, and leadership in creation of academic environments promoting high-quality teaching and research.

Dr. Meindl is a Fellow of the American Association for the Advancement of Science, and a member of the American Academy of Arts and Sciences and the National Academy of Engineering and its Academic Advisory Board. He received the 1999 SIA University Researcher Award, the 1997 Hamerschlag Distinguished Alumnus Award from Carnegie-Mellon University, and the 1991 Benjamin Garver Lamme Medal from ASEE. He was the recipient of the 1990 IEEE Education Medal "for establishment of a pioneering academic program for the fabrication and application of integrated circuits" and the recipient of the 1989 IEEE Solid-State Circuits Medal for contributions to solid-state circuit technology. At the 1988 IEEE International Solid-State Circuits Conference, he received the Beatrice K. Winner Award. In 1980, he was the recipient of the IEEE Electron Devices Society's J.J. Ebers Award for his contributions to the field of medical electronics and for his research and teaching in solid-state electronics. From 1970 through 1978, he and his students received five outstanding paper awards at IEEE International Solid-State Circuits Conferences, along with one received at the 1985 IEEE VLSI Multilevel Interconnections Conference.